Glass Technol.: Eur. J. Glass Sci. Technol. A, December 2011, **52** (6), 190–196

Flexural strength of PVD coated float glass for architectural applications

Robert Meszaros,[1] *Michael Wild,*[2] *Benoit Merle*[3] *& Lothar Wondraczek*[1,4,*]

[1] *Institute of Glass and Ceramics, Department of Materials Science, University of Erlangen-Nuremberg, 91058 Erlangen, Germany*
[2] *Interpane Glasgesellschaft mbH, 94447 Plattling, Germany*
[3] *Institute of General Materials Properties, Department of Materials Science, University of Erlangen-Nuremberg, 91058 Erlangen, Germany*
[4] *Energie Campus Nürnberg, 90403 Nuremberg, Germany*

Manuscript received 24 May 2011
Revision received 30 June 2011
Manuscript accepted 30 June 2011

The effect of PVD coatings on the ring-on-ring flexural strength of soda lime silica float glass was studied. A 70% increase from 280±8 to 478±10 MPa was observed on the air-side of the glass after applying a multilayer low emissivity coating of 100 nm total thickness. A similar but less pronounced effect could be obtained with a TiO_2 single layer of 50 nm. At the same time, for both coatings, the Weibull modulus was found to approximately double. Results are interpreted on the basis of two assumptions: initial defects on the glass surface are covered by the coating, and their growth is prevented due to the protective function of the coating, especially as a humidity barrier. Both assumptions were confirmed by atomic force microscopy and micromechanical analyses. This barrier function leads to significantly improved resistance to long term fatigue and stress corrosion, respectively.

1. Introduction

While glasses count among the intrinsically strongest synthetic materials.[(1)] their practical strength is largely determined by the presence of surface flaws.[(2–4)] Such flaws may occur on various length scales, from macroscopic scratches to, ultimately, topological heterogeneity which may be pertinent to the glass itself.[(5)] They may originate from numerous sources such as forming and handling processes, corrosion and subcritical growth of smaller flaws, especially in the presence of water.[(6–9)] Since avoiding the typical sources of flaws is largely impossible, much effort is presently being put into strategies to improve the defect resistance and/or toughness of glasses for large-scale applications. Such strategies may comprise thermal and chemical tempering (toughening),[(10–13)] (thermal) polishing and etching[(14–16)] or the deposition of permanent coatings or glazes.[(17–23)] The latter are usually based on sol-gel processes, chemical vapour deposition and epoxy or colloidal systems. The actual mechanism which underlies the increase in mechanical strength after coating deposition is often not unambiguously clear because it typically comprises a convolution of effects, from defect coverage, crack tip blunting, corrosion protection and alteration of surface hardness to the creation of residual stresses.

In reality, the applicability of coating procedures to improve the mechanical performance of glasses is largely limited by cost. This limit can most effectively be overcome if coatings which are already applied to glass for a given application can be designed to additionally provide toughening functions. In this respect, the present study is focussed on the effects of physical vapour deposited (PVD) coatings on the mechanical properties of glasses for architectural applications, where PVD coatings are deposited on soda–lime–silica (SLS) float glass on a large scale. The primary purpose of such coatings is to generate specific spectral reflectivity. Typical applications are low emissivity (low-E) and solar protection as shown for example in Figure 1. Both types of coatings are

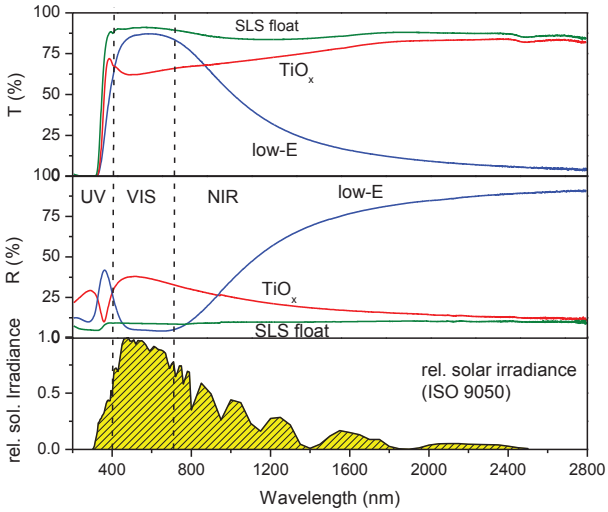

Figure 1. Spectral reflectance and transmission of low-E, TiO_x and uncoated SLS float glass. The relative solar spectral irradiance according to ISO 9050 is shown for comparison

* Corresponding author. Email lothar.wondraczek@ww.uni-erlangen.de

commonly deposited by magnetron sputtering on glass panes of >10 m^2 in size.[24,25] The optical functionality of such coatings is well understood and can be engineered in various fashions.[26] While it is, in principle, known that thin PVD coatings may increase practical strength of a glass,[27] only very few studies quantitatively describe the mechanical properties of sputtered PVD coatings.[27,28] Knowledge of their effect on the mechanical behaviour of architectural glazings and, hence, potential for optimisation is still unsatisfactory. The present study was motivated by the observation which is summarised in Figure 2: in a parallel series of experiments on the lifetime optical performance of low-E glasses, a strong dependence of the evolution of flexural strength with time on the presence of a coating was observed after long term storage in various atmospheres. In addition to a general increase in overall mechanical performance, the continuous decrease in flexural strength, typically a sign of surface corrosion, could be effectively overcome in the presence of a PVD coating. This clearly indicated the protective function of the PVD layer and motivated the present study.

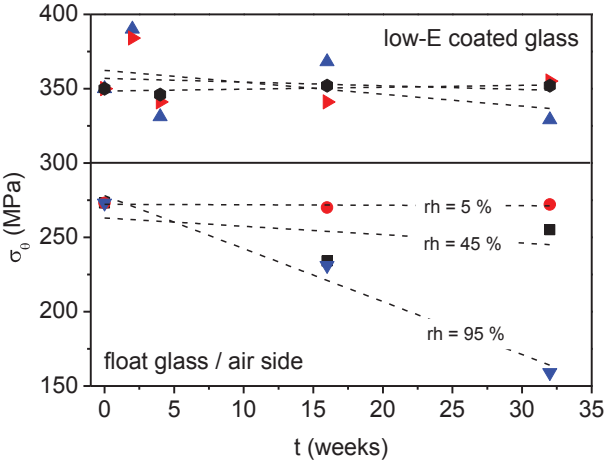

Figure 2. Evolution of ring-on-ring flexural strength of the air-side of SLS float glass with and without a low-E coating during 32 weeks of storage at 5, 45 and 95% relative humidity, respectively. Lines are guides for the eye

2. Experimental

2.1. General

All analyses were performed on as-received commercial SLS float glass (f-glass GmbH, Sülzetal, Germany) with a thickness of 3·8±0·05 mm, density ρ of 2·50±0·01 g/cm^3, Young's modulus E of 71±1 GPa and Poisson's ratio ν of 0·23. A sufficiently large batch of sheet was provided from a single melting-forming campaign so that all glasses had the same age and, it was assumed, identical surface properties. From this batch, coated as well as, for reference, un-coated samples were produced.

2.2 PVD coating procedure

PVD coatings were applied on a 400×1000 mm sheet (~3 m/min) on an industrial magnetron sputtering line (Interpane, Plattling, Germany). Conditioning of as-received plates was performed in a flat glass washing machine using roller brushes, demineralised water and an air knife for subsequent drying. The coating process involved a horizontal in line coater, comprising a series of individual sputtering cathodes (HIPCO, Interpane Entwicklungs- und Beratungsgesellschaft, Lauenförde, Germany). In this way, various multi- and single layer coatings were deposited. Here, we focus on two exemplary types of coatings: a conventional low emissivity (low-E) soft coating for architectural applications and a titanium oxide single layer of 50 nm thickness. Both types of coatings were deposited on the air side of the float glass. The low-E coating comprised a stack of TiO_2 (~25 nm), adhesion interlayers of metallic alloys (~5 nm), Ag (~10 nm), and a top stack of various metal oxides (~50 nm). Titanium oxide films were sputtered from a substoichiometric TiO_x (x=1·6–1·8) ceramic target. For reactive sputtering, oxygen and argon were used as sputter gases at a process pressure of 2–4×10^{-3} mbar.

2.3. Strength tests

Ring-on-ring tests were performed according to DIN EN ISO 1288-5 to determine the biaxial flexural strength of coated, un-coated and corroded specimens. Each test series was conducted on 18–25 specimens, using two different ring configurations (carbon steel) on a universal mechanical testing machine (Instron 4204, Instron Corporation, Texas, USA). Load and support ring diameters were 5 and 22 mm (configuration 'a'), and 8 and 35 mm (configuration 'b'). The load was controlled with a 50 kN load cell at a constant cross-head displacement rate of 0·5 mm/min. Analyses were carried out at room temperature and constant relative humidity. Thin silicone foils (0·2 mm) were placed between the load rings and the glass to ensure homogeneous sample contact. Individual measurements were carried-out on quadratic specimens with edge length l=60±0·8 mm (ring configuration 'a') and l=100±1·5 mm (b), respectively. To exclude edge failure, all edges of each sample were coated with a thick silane layer. The flexural strength σ was then calculated using

$$\sigma = \frac{F}{t^2}\frac{3(1+\nu)}{2\pi}\left[\ln\frac{d_1}{d_2} + \frac{(1-\nu)}{(1+\nu)}\frac{d_1^2 - d_2^2}{2d_3^2}\right] \quad (1)$$

where

$$d_3 = \frac{l\left(1+\sqrt{2}\right)}{2} \quad (2)$$

and F is the applied force at failure, t the thickness

of the specimen, d_1 the diameter of the support ring and d_2 the diameter of the load ring. For each series of strength data, failure probability and Weibull modulus m were calculated.[29] To account for the experimental dependence of strength on specimen size, the effective area A_{eff}, was estimated using[30,31,32]

$$A_{\text{eff}} = \frac{\pi}{2} d_1^2 \left\{ 1 + \left[\frac{4(1+\nu)}{3(1+m)} \right] \left[\frac{5+m}{2+m} \right] \left(\frac{d_2 - d_1}{d_2 d_3} \right)^2 \right\} \times \left[\frac{2d_3^2 (1+\nu) + (d_2 - d_1)^2 (1-\nu)}{(3+\nu)(1+3\nu)} \right] \quad (3)$$

A_{eff} represents a measure of the tested area of the glass sample as a function of ring configuration. It scales the ring-on-ring test to a conventional tensile test and, hence, reflects the probability to encounter a critical flaw on a specimen of a given size.

2.4. Corrosion experiments

In a comparative set of experiments, the impact of storage in a humid environment on experimental strength was analysed. For that, sheet of 20×20 cm² were stored at room temperature for 4, 16 and 32 weeks in relative humidities of 5, 45 and 95%. Low and high humidity values were controlled with silica gel and supersaturated potassium sulphate solution, respectively. The humidity value of 45% was generated in an air conditioned room. After exposure, samples were cut to a size of 50×50 mm² and immediately subjected to ring-on-ring tests as described above.

2.5. Surface characterisation

The surface topography of coated, uncoated and corroded samples was examined by atomic force microscopy (AFM, Veeco Dimension 3100, Veeco instruments, NY, USA) in tapping mode under ambient conditions, using silicon tips with a nominal tip radius of 6 nm (NT-MDT, NSG10/50). AFM scans were recorded at different sample locations over areas of 5×5 μm² and 1×1 μm², respectively, at a scan rate of 1 Hz, a drive frequency of 253 kHz, a tip velocity of 2 μm/s and a force constant of 0·08 N/m. Images were processed using the Gwyddion 2·22 software package.[33]

Mechanical properties of sample surfaces were studied using Vickers micro- and Berkovich dynamic nano-indentation experiments from which hardness, elastic modulus and fracture toughness were derived. Vickers indentation measurements were conducted by applying an indentation load P of 9·81 N for 10 s according to DIN EN ISO 6507. For comparison, additional measurements were made applying a load of 4·91 N. On each specimen, 20 indents were produced and evaluated. The indentation fracture toughness K_{Ic} was calculated from the cracks generated round each indent, assuming halfpenny (radial) cracking, using

$$K_{\text{Ic}} = \eta \left(\frac{E}{H_{\text{V}}} \right)^2 \frac{P}{c^{3/2}} \quad (4)$$

where H_V is the Vickers hardness, c is the semi-circular median radial crack length and η is a dimensionless calibration factor. For silicate glasses, η=0·016±0·004.[34–36] The critical flaw size a was then formally calculated from the characteristic flexural strength σ_θ

$$\sigma_\theta = \frac{K_{\text{Ic}}}{Y\sqrt{a}} \quad (5)$$

where Y *is* a geometrical factor equal to $2{\cdot}24/\pi^{1/2}$ for half-penny cracks. It should be noted that the Vickers indentation fracture toughness test, however, can provide only an estimate of K_{Ic}.[37]

Dynamic nanoindentation measurements (Nano Indenter XP, MTS Nano Instruments, Oak Ridge, USA) were conducted according to the Oliver-Pharr method,[38] providing a qualitative, depth resolved estimate of stiffness. The load was applied with an oscillation frequency of 45 Hz and an oscillation amplitude of 2 nm. The maximum indentation depth h was 200 nm. For each experiment, 50 indents were produced on an area 2×10^4 μm². The size and shape of the indents was analysed immediately after indentation by optical microscopy (Universal Microscope, Olympus BX51, Hamburg, Germany), scanning electron microscopy (ESEM, Quanta 200, FEI, Prague, Czech Republic) and AFM. Indentation data were corrected by the tip area function for indentation depths <200 nm.

3. Results and discussion

3.1. Flexural strength of coated and uncoated samples

In line with previous studies,[30,39,40] a characteristic Weibull flexural strength σ_Θ of the as-received SLS float glass of 280±8 MPa (air side) and 235±12 MPa (tin side), respectively, was obtained. Within the considered experimental range, these values did not depend on the employed ring geometry and, hence, tested area. Data are shown in Figures 3–4. The somewhat lower characteristic strength of the tin side is well documented in literature.[30,40,41] Weibull modulii (90% confidence interval) were 3·3±0·3 and 5·4±0·2, respectively. Estimated effective areas were 343±87 mm² for the tin side and 483±115 mm² for the air side (ring configuration 'a') and 848±208 mm² and 1047±261 mm², respectively (ring configuration 'b', Table 1). The differences in A_{eff} between tin side and air side result from different values of m and, hence, different flaw size distributions. The absolute characteristic flexural strength of the glass was found to increase by more than 70% when a multilayer low-E coating was applied to the air side (Figures 3 and 4). That is, σ_Θ=478±10 MPa and m=5·4±0·6 (90%

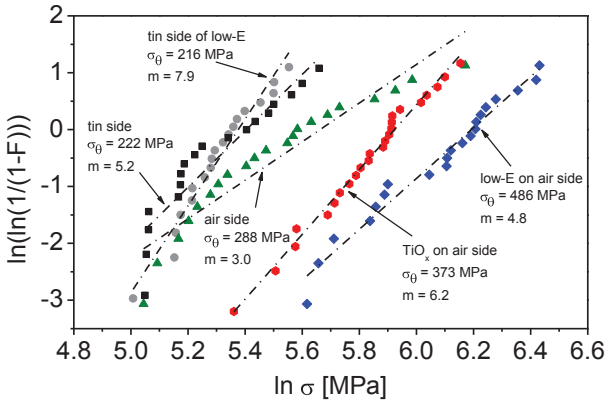

Figure 3. Weibull distribution of ring-on-ring flexural strength of coated (air- and tin-side) and uncoated SLS float glasses (coating on air-side, ring configuration "a")

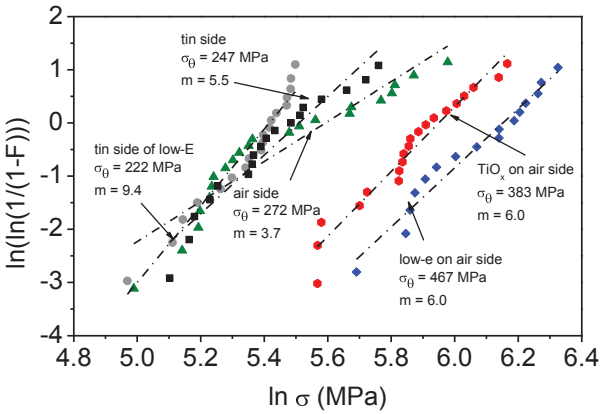

Figure 4. Weibull distribution of ring-on-ring flexural strength of coated (air- and tin-side) and uncoated SLS float glasses (coating on air-side, ring configuration "b")

confidence interval, Table 1, air side of low-*E* coated glass). A somewhat lower increase was observed when the single layer of TiO_2 was applied (σ_Θ=378±5 MPa, *m*=6·1±0·1). This indicates that the ultimate mechanical performance of the low-*E* coated glass is either determined by the thin top layers which were deposited onto the 25 nm intermediate TiO_2 coating, or by the presence of interfaces with various degrees of plasticity. Interestingly, the uncoated tin-side of low-*E* as well as TiO_2 coated glasses exhibited slightly lower σ_Θ and significantly higher *m* as compared to as-received SLS float glass (Table 1). This reflects a more uniform distribution of critical flaws. which may be a result of contact damage induced on the tin-side of the glass by the transport rollers inside the PVD-coating line. Noteworthy, *post mortem* analysis of fracture patterns clearly confirmed that in all cases, fracture originated in the centre of the samples. Due to the higher load at fracture, coating-side-tested glasses fractured into significantly smaller fragments (Figure 5).

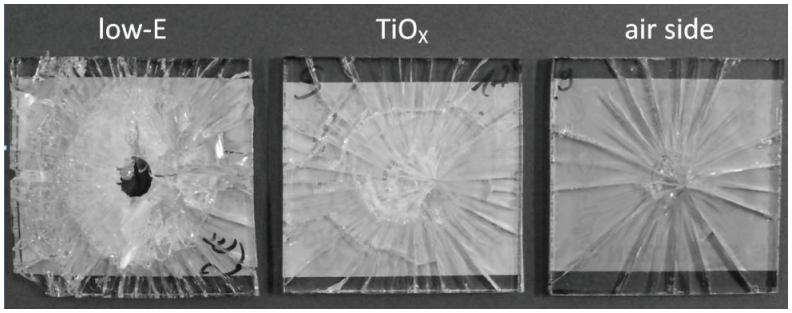

Figure 5. Fracture pattern after ring-on-ring flexural testing of the air-sides of coated and uncoated SLS float glass

Table 1. Ring-on-ring characteristic flexural strength σ_Θ*, Weibull modulus m and effective area* A_{eff} *of tin- and air-side of coated and uncoated SLS float glass. Values in the parenthesis represent the 90% -confidence interval for* n *specimens*

Test	n	σ_θ *(MPa)*	m	A_{eff} *(mm2)*
RoR configuration (a)				
tin side	18	222 [198; 247]	5·2 [3·2; 7·2]	343 [289 ;463]
air side	21	288 [244; 339]	3·0 [2·1; 4·3]	483 [384; 613]
low-E on air side	21	486 [437; 539]	4·8 [3·3; 6·9]	360 [295; 454]
tin side of low-E	19	216 [201; 232]	7·9 [4·9; 11·1]	277 [240; 355]
TiOx on air side	24	373 [213; 471]	6·2 [4·1; 8·2]	312 [272; 396]
RoR configuration (b)				
tin side	18	247 [222; 274]	5·5 [3·4; 7·6]	848 [718;1134]
air side	21	272 [238; 311]	3·7 [2·5; 5·3]	1047 [865;1387]
low-E on air side	16	467 [425; 513]	6·0 [3·9; 9·2]	809 [659;1039]
tin side of low-E	18	222 [211; 236]	9·4 [6·4; 13·8]	653 [568; 782]
TiOx on air side	20	383 [351; 417]	6·0 [4·1; 8·7]	809 [675;1007]

3.2. Surface topology

The most obvious origin of increasing practical strength after coating deposition is covering of surface flaws and/or crack blunting. AFM analyses were therefore carried out to evaluate surface topology before and after coating. Data are summarised in

Table 2. Vickers micro-hardness H_V*, fracture toughness* K_{Ic}*, average critical flaw size* a*, average rms roughness and maximum z-contrast* h_{max} *of tin- and air-side of coated and uncoated SLS float glass*

Test	$H_{V\,4\text{-}9N}$ *(GPa)*	$H_{V\,9\text{-}8N}$ *(GPa)*	K_{Ic} *(kNm$^{1/2}$)*	a *(μm)*	*rms 1 μm² (nm)*	*rms 25 μm² (nm)*	h_{max} *25 μm² (nm)*
tin side	6·29	6·35	0·67	5·2	0·25	0·28	2·58
air side	6·08	6·34	0·70	3·9	1·46	1·87	48·50
low-E on air side	6·93	8·73	0·67	1·9	1·15	1·18	10·39
TiO_x on air side	6·89	7·44	0·70	2·2	0·48	0·54	5·40

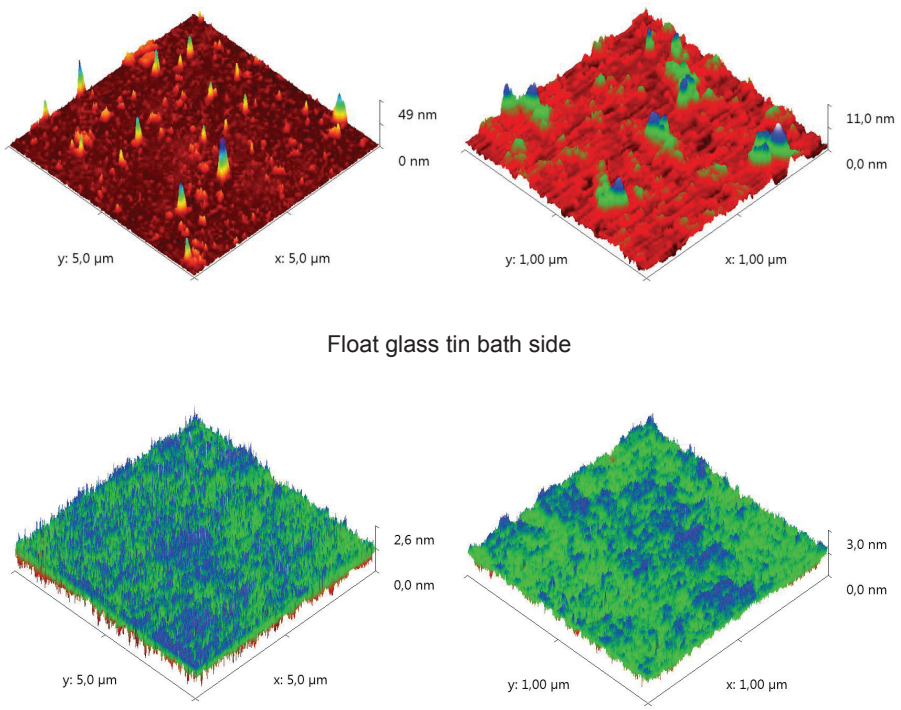

Figure 6. Effective hardness and Young's modulus (inset) as a function of indentation depth for low-E and TiO_2 coated SLS float glass respectively (air-side), as obtained by Berkovich-nanoindentation

Table 2. An example surface scan of the as received SLS float glass is shown in Figure 6. Over an area of 5×5 µm^2, data revealed the presence of regularly distributed features with a z-dimension of 48 nm on the air-side. Ignoring these features, a root mean square roughness (rms-roughness) of 1·9 nm was found. For a scan size of 1×1 µm^2, individual features of ~9 nm in z-dimension were found at otherwise similar *rms*-roughness. In comparison, the tin-side appears significantly smoother with a rms-roughness of about 0·27 nm for the same scan size. Notable spikes are not visible in this case. AFM analyses of coated surfaces are shown in Figure 7. For the low-E coating, the rms-roughness was found to be 1·18 nm (5×5 µm^2). Again, the sharp spikes which were seen on the uncoated air-side are not visible on the coated specimen. Maximum

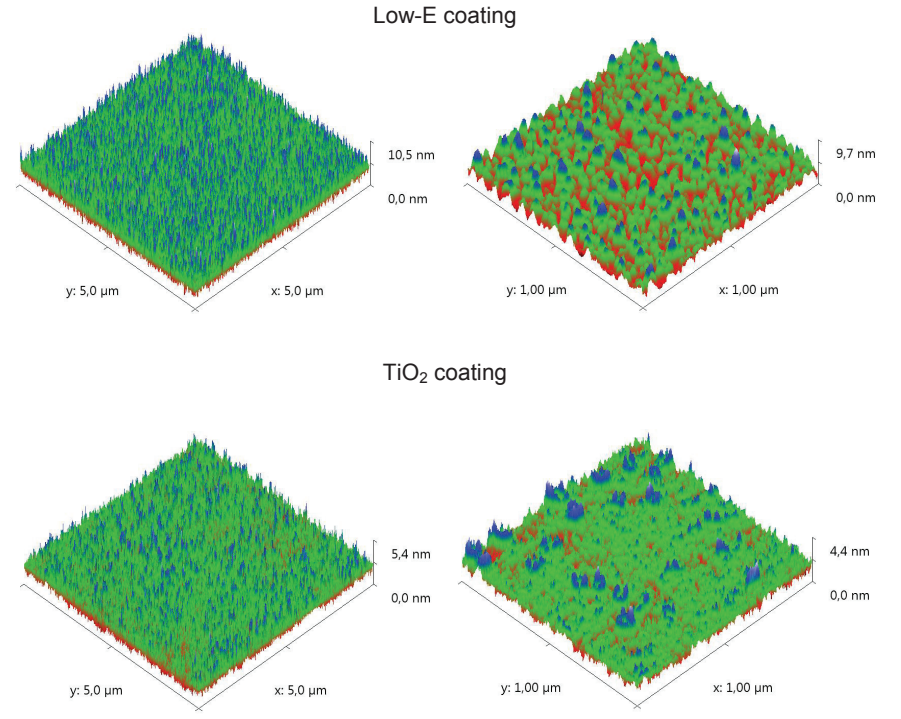

Figure 7. AFM topographical images of the air and tin side of the as received soda lime silica float glass at two scales (5×5 µm and 1×1 µm)

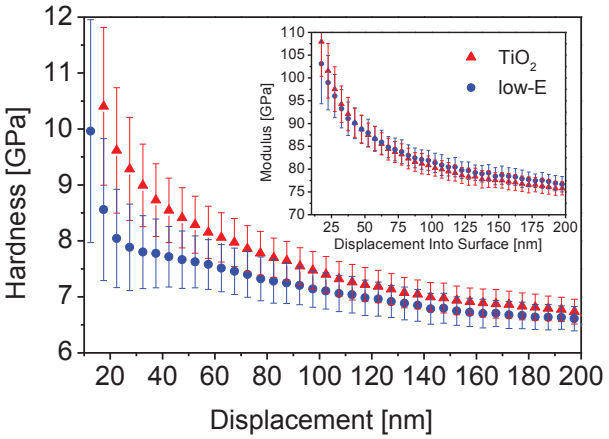

Figure 8. AFM topographical images of low-E and TiO_x coated air side of soda lime silica float glass at two scales (5×5 μm and 1×1 μm).

z-contrast was 10 nm. Considering the thickness of the low-E coating of ~100 nm, one may assume that smaller features which are found on the uncoated glass surface were covered during the coating process. As for the larger features, it is further assumed that they are the result of early-stage corrosion of the uncoated glass which was effectively avoided by the presence of the coating. That is, the larger features were not covered by the coating, but their occurrence was avoided altogether. Similar results were found for the TiO_2 single layer (Table 2).

3.3. Surface hardness

Values of Vickers indentation hardness of coated and uncoated are summarised in Table 2. Average hardness values of 6·3 and 6·2 GPa were obtained for tin-side and air-side, respectively. For the coated samples, apparent hardness depended significantly on the applied load, i.e. 6·9 GPa for a load of 4·91 N and 8·7 GPa for a load of 9·81 N for the low-*E* coating and similarly 6·9 GPa for a load of 4·91 N and 7·4 GPa for a load of 9·81 N for the TiO_2-coating. Average penetration depths were 7·5 μm for 4·9 N applied indentation load and 11·5 μm for 9·8 N, respectively. Figure 8 represents dynamic nanoindentation experiments performed on low-*E* and TiO_2 coated SLS float glass (air-side). Data represent apparent values of hardness and Young's modulus, integrated over coating and substrate with progressing indentation depth. The complex coating architecture (low-*E*) and comparably low coating thickness allow only qualitative conclusions. For an indentation depth of >100 nm, the data obtained are largely determined by the glass substrate. For the considered coating thickness, substrate effects may be neglected only for the first 10–30 nm.[42] The data clearly indicate higher hardness for the TiO_2 single layer, and a dissipative effect which may be due to the Ag interlayer for the low-*E* coating. Both coatings exhibit similar elastic modulus of ~100 GPa compared to the modulus of SLS of ~70 GPa. Data also show increasing experimental uncertainty with decreasing indentation depth which may be due to the geometry of the indenter and the related difficulties in applying the appropriate tip area function.[43] When the indentation depth exceeds about 200 nm, hardness of both types of coated samples converges to about 6·5 GPa. This value is in good agreement with the microscopic Vickers experiment.

The fracture toughness K_{Ic} was calculated from the median radial crack length generated by Vickers microindentation (no cracks could be found after nanoindentation for indentation depths <3 μm). For 60% of the Vickers indents, halfpenny cracks were observed. From these, a value of 0·68±0·15 MPa $m^{1/2}$ was obtained for K_{Ic} for all specimens, independent on the presence of a coating. This value corresponds well to literature data (typically $0{\cdot}65<K_{Ic}<0{\cdot}8$ MPa $m^{1/2}$ under ambient conditions[34,44,45]). From this, the critical flaw size *a* was calculated, confirming the above discussion (Table 2).

5. Conclusions

In summary, the effect of PVD coatings on the ring-on-ring flexural strength of SLS float glass was studied. A 70% increase, i.e. from 280±8 to 478±10 MPa was observed on the air-side of the glass after applying a multilayer low-*E* coating. A similar but less pronounced effect could be obtained with a TiO_2 single layer of 50 nm. At the same time, the Weibull modulus was found to approximately double for both coatings. Results are interpreted on the basis of two assumptions: initial defects on the glass surface are covered by the coating, and defect propagation is prevented due to the protective function of the coating, especially as a humidity barrier. Both assumptions were confirmed by AFM and micromechanical analyses. Interestingly, this leads to significantly improved resistance to long term fatigue and stress corrosion.

Acknowledgement

The authors gratefully acknowledge financial support from the Bayerische Forschungsstiftung through the program FORGLAS - Glasses for energy-efficient building technologies.

References

1. Kurkjian, C. R., Gupta, P. K., Brow, R. K. & Lower, N. "The intrinsic strength and fatigue of oxide glasses. *J. Non-Cryst. Solids*, 2003, **316** (1), 114–24.
2. Griffith, A. A. The phenomena of rupture and flow in solids. *Philos. Trans. Royal Soc. London. Series A*, 1921, 163–98.
3. Shand, E. B. Strength of glass—the Griffith method revised. *J. Am. Ceram. Soc.*, 1965, **48** (1), 43–9.
4. Wondraczek, L., Deubener, J., Eckert, J., Horbach, J. & Mauro, J. C. Towards ultrastrong glasses. *Adv. Mater.* , 2011, communicated.
5. Champagnon, B., Wondraczek, L. . & Deschamps, T. Boson peak,

structural inhomogeneity, light scattering and transparency of silicate glasses. *J. Non-Cryst Solids,* 2009, **355** (10–12), 712–14 .
6. Wondraczek, L., Dittmar, A., Oelgardt, C., Célarié, F., Ciccotti, M. & Marlière, C. Real-time observation of a non-equilibrium liquid condensate confined at censile crack tips in oxide glasses. *J. Am. Ceram. Soc.,* 2006, **89** (2), 746–9.
7. Ciccotti, M., George, M., Ranieri, V., Wondraczek, L. & Marlière, C. Dynamic condensation of water at crack tips in fused silica glass. *J. Non-Cryst. Solids*, 2008, **354** (2–9), 564–68.
8. Adams, R. & McMillan, P. W. The decoration of surface flaws in glass. *J. Mater. Sci,* 1977, **12** (12), 2544–6.
9. Freiman, S. W., White, G. S. & Fuller, Jnr., E. R. Environmentally enhanced crack growth in soda-lime glass. *J. Am. Ceram. Soc.,* 1985, **68** (3), 108–12.
10. Sugarman, B. Strength of glass (a review). *J. Mater. Sci.,* 1967, **2** (3), 275–83.
11. Zijlstra, A. L. & Burggraaf, A. J. Fracture phenomena and strength properties of chemically and physically strengthened glass. Part 1. General survey of strength and fracture behaviour of strengthened glass. *J. Non-Cryst. Solids,* 1968, **1** (1), 49–68.
12. Zijlstra, A. L. & Burggraaf, A. J. Fracture phenomena and strength properties of chemically and physically strengthened glass. Part 2. Strength and fracture behaviour of chemically strengthened glass in connection with the stress profile. *J. Non-Cryst. Solids,* 1969, **1** (2), 163–85.
13. Karlsson, S., Jonson, B. & Stalhandske, C. The technology of chemical glass strengthening - a review. *Glass Technol.: Eur. J. Glass Sci. Technol. Part A*, 2010, **51** (2), 41–54.
14. Kolli, M., Hamidouche, M., Bouaouadja, N. & Fantozzi, G. HF etching effect on sandblasted soda-lime glass properties. *J. Eur. Ceram. Soc.,* 2009, **29** (13), 2697–704.
15. Wereszczak, A. A., Harper, D. C., Duty, C. E. & Patel, P. Glass strengthening via high-intensity plasma-arc heating. *J. Am. Ceram. Soc.,* 2010, **93** (5), 1256–9.
16. Sozanski, M. R. & Varshneya, A. K. Strengthening of glass tubes and containers by flame-sprayed glazing. *Am. Ceram. Soc. Bull.,* 1987, **66** (11), 1630–4.
17. Verganelakis, V., Nicolaou, P. D. & Kordas, G. Processing and properties of glass strengthened by Ormosil coatings. *Glass Technol.*, 2000, **41** (1), 22–9.
18. Shi, Z. M. & Ji, G. J. A method to improve mechanical properties of glass plates by surface-coating titania nanofilms with sol-gel technique. *Surf. Coatings Technol.*, 2008, **202** (8), 1350–6.
19. Hand, R. J., Ellis, B., Whittle, B. R. & Wang, F. H. Epoxy based coatings on glass: strengthening mechanisms. *J. Non-Cryst. Solids*, 2003, **315** (3), 276–87.
20. Fabes, B. D. & Uhlmann, D. R. Strengthening of glass by sol-gel coatings. *J. Am. Ceram. Soc.,* 1990, **73** (4), 978–88.
21. Brzesowsky, R. H., De With, G., Van Den Cruijsem, S., Snijkers-Hendrickx, I. J. M., Wolter, W. A. M. & Van Lierop, J. G. Glass strengthening by silica particle reinforced organic-inorganic coatings. *J. Non-Cryst. Solids*, 1998, **241** (1), 27–37.
22. Carturan, G., Khandelwal, N., Tognana, L. & Sglavo, V. M. Strengthening of soda-lime-silica glass by surface treatment with sol-gel silica. *J. Non-Cryst. Solids*, 2007, **353** (16–17), 1540–5.
23. Briard, R., Heitz, C. & Barthel, E. Crack bridging mechanism for glass strengthening by organosilane water-based coatings. *J. Non-Cryst. Solids*, 2005, **351** (4), 323–30.
24. Beister, G., Dietrich, E., Schaefer, C., Scherer, M. & Szczyrbowski, J. Progress in large-area glass coatings by high-rate sputtering. *Surf. Coatings Technol.*, 1995, **76–77** (Part 2), 776–85.
25. Greenberg, C. B. Thin films on float glass: the extraordinary possibilities. *Ind. Eng. Chem. Res.*, 2000, **40** (1), 26–32.
26. Arbab, M. & Finley, J. J. Glass in architecture. *Int. J. Appl. Glass Sci.*, 2010, **1** (1), 118–29.
27. Chen, J. & Bull, S. J. Indentation fracture and toughness assessment for thin optical coatings on glass. *J. Phys. D,* 2007, **40** (18), 5401.
28. Chen, J. & Bull, S. J. Multi-cycling nanoindentation study on thin optical coatings on glass. *J. Phys D*, 2008, **41** (7), 074009.
29. Weibull, W. A statistical distribution function of wide applicability. *J. Appl. Mech. Tran.s ASME*, 1951, **18** (3), 293–7.
30. Wereszczak, A. A., Kirkland, T. P., Ragan, M. E. Strong, K. T. Lin, H.-T. & Patel, P. Size scaling of tensile failure stress in a float soda–lime–silicate glass. *Int. J. Appl. Glass Sci.*, 2010, **1** (2), 143–50.
31. Quinn, G. D. Weibull strength scaling for standardised rectangular flexure specimens. *J. Am. Ceram. Soc.,* 2003, **86** (3), 508–10.
32. Jain, R., Lock, J. & Duffy, S. F. Effective area and effective volume calculations for ceramic test specimens. *ASME Conf. Proc.,* 2009, (48821), 231–9.
33. http://gwyddion.net/ 2011.
34. Dériano, S., Jarry, A., Rouxel, T., Sangleboeuf,, J. C. & Hampshire, S. The indentation fracture toughness (KC) and its parameters: the case of silica-rich glasses. *J. Non-Cryst Solids*, 2004, **344** (1–2), 44–50.
35. Yoshida, S., Hidaka, A. & Matsuoka, J. Crack initiation behavior of sodium aluminosilicate glasses. *J. Non-Cryst. Solids*, 2004, **344** (1–2), 37–43.
36. Cook, R. F. & Pharr, G. M. Direct observation and analysis of indentation cracking in glasses and ceramics. *J. Am. Ceram. Soc.*, 1990, **73** (4), 787–817.
37. Quinn, G. D. & Bradt, R. C. On the Vickers indentation fracture toughness test. *J. Am. Ceram. Soc.*, 2007, **90** (3), 673–80.
38. Oliver, W. C. & Pharr, G. M. Improved technique for determining hardness and elastic modulus using load and displacement sensing indentation experiments. *J. Mater. Res.*, 1992, **7** (6), 1564–80.
39. Fett, T., Rizzi, G., Guin, J. & Wiederhorn, S. Ring-on-ring strength measurements on rectangular glass slides. *J. Mater. Sci.*, 2007, **42** (1), 393–5.
40. Krohn, M. H., Hellmann, J. R., Shelleman, D. L., Pantano, C. G. & Sakoske, G. E. Biaxial Flexure Strength and Dynamic Fatigue of Soda–Lime–Silica Float Glass. *J. Am. Ceram. Soc.*, 2002, **85** (7), 1777–82.
41. Gulati, S. T. Akcakaya, R. & Varner, J. R. Fracture behavior of tin vs. air side of float glass. In: *Fractography of Glasses and Ceramics IV.* Edited by J. R.Varner and G. D. Quinn., Westerville, OH, 2001, 317–25.
42. Howell, J. A., Hellmann, J. R. & Muhlstein, C. L. Nanomechanical properties of commercial float glass. *J. Non-Cryst. Solids*, 2008, **354** (17), 1891–9.
43. Li, X. & Bhushan, B. A review of nanoindentation continuous stiffness measurement technique and its applications. *Mater. Charact.*, 2002, **48** (1), 11–36.
44. Geandier, G., Denis, S. & Mocellin, A. Float glass fracture toughness determination by Hertzian contact: experiments and analysis. *J. Non-Cryst. Solids*, 2003, **318** (3), 284–95.
45. Warren, P. D. Determining the fracture toughness of brittle materials by Hertzian indentation. *J. Eur. Ceram. Soc.*, 1995, **15** (3), 201–7.